Modeling of GaInP/GaAs/Ge and the inverted-grown metamorphic GaInP/GaAs/GaInAs triple-junction solar cells

Y. G. Xiao*, Z. Q. Li, Z. M. Simon Li
Crosslight Software Inc., 121-3989 Henning Drive, Burnaby, BC V5C 6P8 Canada

ABSTRACT

In this work, based on the advanced drift and diffusion theory with improved tunneling junction model, two-dimensional modeling for the GaInP/GaAs/Ge and the inverted-grown metamorphic GaInP/GaAs/GaInAs triple-junction solar cells are performed by using a commercial software, the Crosslight APSYS. Basic physical quantities like band diagram, optical absorption and generation are obtained and characteristic results such as I-V curves, current matching, fill factor, efficiency etc under one-sun and multi-sun illumination are presented. Some of the modeling results generally agree with the published experimental results for both TJ cells. Comparative analyses are made with these two TJ cells and optimization approaches are discussed with respect to minority carrier lifetime, front anti-reflection coating, and top contact grid size and spacing.

Keywords: GaInP/GaAs/Ge triple-junction cell, GaInP/GaAs/GaInAs triple-junction cell, solar cell, solar photovoltaics, device modeling, modeling and CAD software

1. INTRODUCTION

The development of solar cell technology has been continuously advancing due to the search for alternative energy sources. The monolithic, series interconnected multi-junction (MJ) solar cells based on group III-V semiconductor material system (such as GaInP/GaAs) are proven to be very attractive for many space and terrestrial applications[1,2] in replacing the conventional solar cells based on silicon (Si). The MJ solar cells have been demonstrated to be more efficient with better radiation hardness than Si solar cells. These MJ solar cell arrays have been used to provide space power for interplanetary missions such as deep space and Mars lander besides near-earth orbits[3]. High concentration receivers for terrestrial power generation have also been explored[4].

Typical GaInP/GaAs/Ge triple-junction (TJ) solar cells with conversion efficiency over 30% under one sun have been widely achieved, and efficiency in excess of 38.9% for concentration between 100 and 500 suns has been achieved[5]. Recent efforts to enhance conversion efficiency for MJ solar cells are performed with the metamorphic, or lattice-mismatched semiconductor materials. A Ge-free III-V GaInP/GaAs/GaInAs TJ solar cell device structure grown inverted with a metamorphic bottom junction was demonstrated with achieved efficiency 33.8% under one sun and 38.9% under 81 suns[6]. Another metamorphic GaInP/GaInAs/Ge TJ solar cell showed record 40% efficiency under 270 suns[7]. MJ solar cells including 4, 5 and 6 subcells are also being developed[8].

Whereas technological development on solar cell fabrication and panel construction has been advanced during the past years, better modeling methods and software, especially compact packages with full breadth, are increasingly demanded because of their advantages in saving the R&D time and cost and capability in optimizing device design. For the concentrator solar cells, it would be difficult to extract detailed information simply by inspecting the measurement data when more subcells are incorporated to form the complex MJ solar cells with tunnel junctions. Good simulation software could usually help to obtain a better understanding of the performance characteristics and predict the operational condition for these solar cells.

In this work, based on Crosslight's device simulator, the APSYS[9], two-dimensional (2D) simulations have been performed on GaInP/GaAs/Ge and the inverted-grown metamorphic GaInP/GaAs/GaInAs TJ solar cells. This paper is organized as follows. In section 2, the simulator APSYS and basic theoretic background are briefly described. The device structure and simulation details are explained in section 3. Modeling results, analyses and discussion are presented in section 4. Finally, a summary is given in section 5.

*yxiao@crosslight.com; phone: 1-604-320-1704; fax: 1-604-320-1734; www.crosslight.com

High and Low Concentration for Solar Electric Applications III, edited by Martha Symko-Davies,
Proc. of SPIE Vol. 7043, 70430B, (2008) · 0277-786X/08/$18 · doi: 10.1117/12.795576

2. SIMULATOR APSYS AND THEORETIC BACKGROUND

The APSYS simulator[9,10] is a general-purpose 2D/3D finite element analysis and modeling software for semiconductor devices. It includes many advanced physical models and offers a flexible modeling and simulation environment. Advanced features include heterojunction models, (quantum) tunneling, hot carrier transport, trap dynamics, impact ionization and non-isothermal analysis etc. The simulator solves several interwoven equations including the basic Poisson's equation, and drift-diffusion current equations for electrons and holes. Poisson's equation is as follows,

$$-\nabla\cdot\left(\frac{\varepsilon_0\varepsilon_{dc}}{q}\nabla V\right)=-n+p+N_D(1-f_D)-N_A f_A+\sum_j N_{tj}\left(\delta_j-f_{tj}\right) \tag{1}$$

and here the last term describes the deep trap density effect. In the above equation, V is electrical potential, ε_0 vacuum dielectric constant, ε_{dc} relative DC or low frequency dielectric constant, q electronic charge, n electron concentration, p hole concentration, N_D the shallow donor density, N_A the shallow acceptor density, f_D occupancy of the donor level, f_A occupancy of the acceptor level, N_{tj} the density of the jth deep trap, f_{tj} the occupancy of the jth deep trap level, and δ_j is 1 for donor-like traps and 0 for acceptor-like traps. The current continuity equations for electrons and holes are respectively expressed as

$$\nabla\cdot J_n-\sum_j R_n^{tj}-R_{sp}-R_{st}-R_{au}+G_{opt}(t)=\frac{\partial n}{\partial t}+N_D\frac{\partial f_D}{\partial t}, \tag{2}$$

$$\nabla\cdot J_p+\sum_j R_p^{tj}+R_{sp}+R_{st}+R_{au}-G_{opt}(t)=-\frac{\partial p}{\partial t}+N_A\frac{\partial f_A}{\partial t}. \tag{3}$$

Here J_n and J_p are electron and hole current flux density respectively. R_n^{tj} and R_p^{tj} are electron and hole recombination rates per unit volume through the jth deep trap respectively. G_{opt} is the optic generation rate, R_{sp}, R_{st}, and R_{au} the spontaneous recombination rate, the stimulated recombination rate and the Auger recombination rate per unit volume respectively. These equations govern the electrical behavior (e.g., I-V characteristics) of a semiconductor device.

Since it is difficult to introduce all the models and equations for the simulator APSYS, here only some of them are briefly described. Among them, bandgap narrowing effect needs to be mentioned. It is observed experimentally that the shrinkage of bandgap occurs when impurity concentration is particularly high, e.g. $n_{imp}> 10^{23}$ m^{-3}. This is so called bandgap narrowing effect which is ascribed to the emerging of the impurity band formed by the overlapped impurity states. The bandgap narrowing model can be expressed as

$$\Delta E_g = E_{ref}\left\{\ln\frac{n_{imp}}{n_{ref}}+\sqrt{\ln^2\frac{n_{imp}}{n_{ref}}+0.5}\right\} \tag{4}$$

where E_{ref}, n_{ref} and n_{imp} represent energy parameter, density parameter and impurity concentration, respectively.

The carrier mobilities μ_n and μ_p account for the scattering mechanism for electrical transport. The software simulator provides several mobility model options, from constant values to field dependant ones. A commonly used mobility model has the following form for electrons and holes respectively.

$$\mu_n=\frac{\mu_{0n}}{\left[1+\left(\mu_{0n}F/v_{sn}\right)^{\beta_n}\right]^{1/\beta_n}} \qquad \mu_p=\frac{\mu_{0p}}{\left[1+\left(\mu_{0p}F/v_{sp}\right)^{\beta_p}\right]^{1/\beta_p}} \tag{5}$$

Here F is the electric field, v_{sn} and v_{sp} the saturation velocity for electron and hole, μ_{0n} and μ_{0p} the low field electron and hole mobilities, and β_n and β_p constant values corresponding to electron and hole respectively. The simulator also provides an option to include the impurity dependence of the low field mobility.

Tunnel junctions play an important role in the MJ solar cells by facilitating the current transfer from one subcell to another. A thin tunnel junction could be simply created by doping either side of the junction very heavily. If both sides of the junction are sufficiently doped, the conduction band and valence bands may cross the Fermi level to align the electrons with empty states. The simulator provides a more complex Zener-type tunneling where the newly tunneling created carriers can lead to impact ionization when drifting in the strong electric field region. Following the band-to-band tunneling in Refs.[11-13], the tunneling probability is solved by WKB approximation and expressed as follows.

$$D = \exp\left(-2J\left(E_{\parallel}\right)\right) = P_0 \exp\left(-E_{\perp}/\underline{E}\right) \tag{6}$$

$$J\left(E_{\parallel}\right) = \int_{x_1}^{x_2} \left| \left(2m^*/\hbar^2\right)\left[\left(E_g/2\right)^2 - \varepsilon_c{}^2\right]/E_g + E_{\perp} \right|^{\frac{1}{2}} dx \tag{7}$$

$$P_0 = \exp\left[\frac{\pi m^{*1/2}\left(E_g\right)^{3/2}}{2(2)^{1/2} qF\hbar}\right] = \exp\left(-\frac{E_g}{4\underline{E}}\right) \tag{8}$$

$$\underline{E} = \frac{2^{1/2} qF\hbar}{2\pi m^{*1/2}\left(E_g\right)^{1/2}} \tag{9}$$

Here $E_{\parallel}$ and $E_{\perp}$ are electron kinetic energy in the direction parallel and perpendicular to the tunneling direction, respectively. $\underline{E}$ is the measure of significance of perpendicular momentum. m^* is the effective tunneling mass. P_0 has the meaning of the tunneling probability with a zero perpendicular momentum. When applying the aforementioned Zener tunneling model to p-n junction diode, the differential current density of a tunneling flow could be expressed approximately as

$$dI/A = q^2 F m^* / \left(2\pi^2\hbar^3\right) P_0 \underline{E} dx \,. \tag{10}$$

An equivalent mobility model can be obtained based on Eq. (10) and used for numerical computation. This enables an efficient modeling of MJ solar cell across the whole solar spectra, where all the spectrum data points are processed by taking into account the effects of multiple layer optical interference and photon generation. For optic simulation related to electron-hole generation due to incident light, the software uses transfer matrix method (TMM)[14] to calculate the light propagation inside the solar cell device by taking into account the reflections at the multi-layer interfaces. Ray-tracing technique is also provided to handle the textured surfaces and non-planar structures.

Most modeling analyses of solar cells are conducted by one-dimensional simulation[15]. However, many important issues in solar cell design have to be studied by advanced 2D/3D simulation. For example, the size and spacing of the contact fingers are crucial to reduce series resistance, and 2D/3D carrier transport simulation is necessary. In thin film solar cells, the non-uniformly distributed deep traps have also to be handled by 2D/3D simulation.

3. DEVICE STRUCTURE AND SIMULATION DETAILS

The device structure for the GaInP/GaAs/Ge TJ cell is similar to the ones in Refs. 16 and 17, and is schematically shown in Fig. 1 (a). As seen from the figure, starting from the bottom, the TJ solar cell is constructed with three subcells, namely Ge, GaAs and GaInP junctions stacked in series. Anti-reflective coating (ARC) is at the very top. The GaAs and GaInP subcell each has a back surface field (BSF) layer at the bottom and a window layer at the top. Two tunnel junctions are implemented and placed between each pair of neighboring subcells. Although the actual device growth uses thin GaAs p^+/n^+ diode as the tunneling junction, for the convenience of modeling, the tunnel junction is replaced as $Al_{0.01}GaAs$ p^+/n^+ junction. All the n-type emitter layers are assumed to be 0.1 μm. The main p-type absorber layers for GaInP, GaAs and Ge are 0.45, 3.5 and 11 μm except for current-matching modeling where the main absorber layer thickness is adjusted. Crosslight APSYS describes the device structure generally with a layer file by a friendly-using LayerBuilder (starting from the bottom substrate usually). Different columns could also be added to describe the more realistic device structure. The so-built layer structure forms a 2D cross section, and the layer view for the investigated TJ solar cell is displayed in Fig. 1 (b). For GaInP/GaAs/Ge TJ cell, the solar spectra used for irradiation is the standard air mass zero (AM0) Solar.AM0[18,19].

The device structure for the metamorphic GaInP/GaAs/GaInAs TJ cell is schematically shown in Fig. 2 (a)[6] and the layer setup is schematically shown in Fig. 2 (b). The monolithic TJ structure was inverted grown on GaAs substrate. The top GaInP and middle GaAs lattice-matched junctions were grown before the bottom metamorphic $Ga_{0.7}In_{0.3}As$ junction to prevent the threading dislocations due to lattice mismatch. The three junctions were series connected with two $Al_{0.3}Ga_{0.7}As$/GaAs tunnel junctions. A graded $Ga_xIn_{1-x}P$ layer ($0.22<x<0.51$), which is transparent to the light for the bottom GaInAs junction, was used to minimize the dislocations in the bottom GaInAs junction. $Ga_{0.3}In_{0.7}P$ composition was used as the window and back-furface-field (BSF) layers for the GaInAs junction. MgF_2/ZnS layers were used as

ARC. All the n-type emitter layers are assumed to be 0.1 μm. The main p-type absorber layers for GaInP, GaAs and GaInAs are 0.9, 2.5 and 2.9 μm except for current-matching modeling where the main absorber layer thickness is adjusted. The solar irradiation used for modeling the inverted metamorphic GaInP/GaAs/GaInAs TJ cell is the standard air mass 1.5 global spectra (AM1.5G[20]) unless specified.

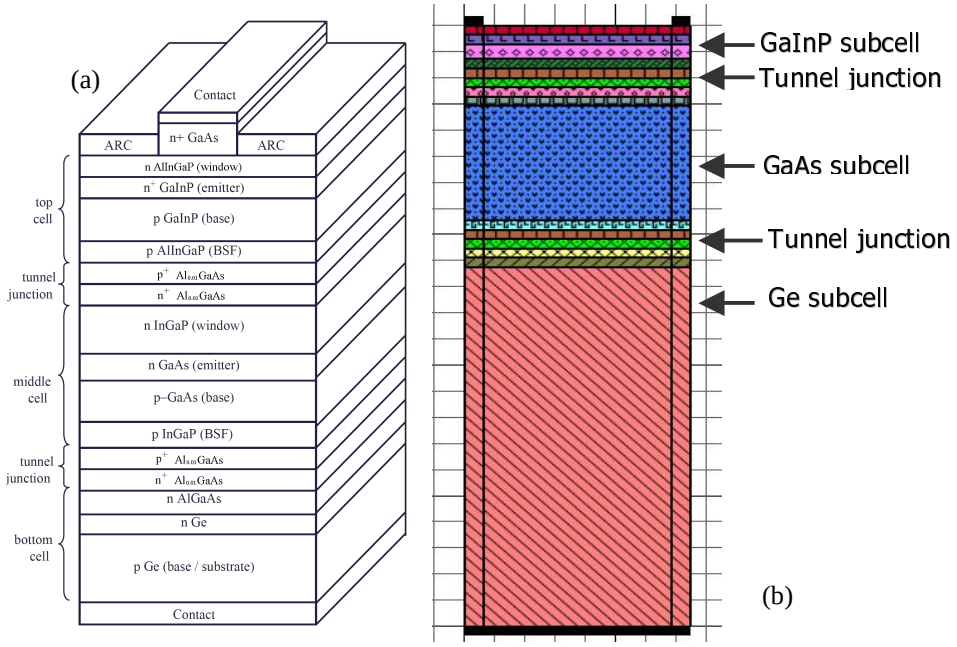

Fig. 1. (a) Schematic GaInP/GaAs/Ge TJ solar cell device structure and (b) schematic layer view generated by Crosslight APSYS simulator.

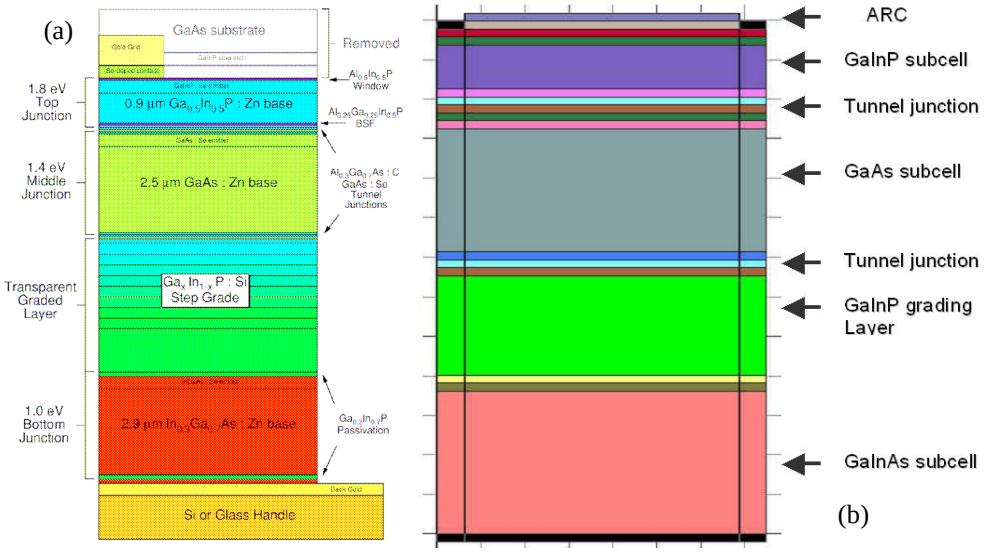

Fig. 2. (a) Schematic GaInP/GaAs/GaInAs TJ solar cell device structure[6] and (b) schematic layer view generated by Crosslight APSYS simulator.

From the layer file, the simulator can generate files for mesh, material and doping information, which will be subsequently cited by the solving file for simulating the device. Besides solar spectra, index files including wavelength dependent refractive index n and extinction coefficient κ for Ge, GaInP, GaAs, GaInAs, MgF_2 and ZnS etc are taken from experiments[21-23]. By using the expression $\alpha = 4\pi\kappa / \lambda$ the absorption coefficients α of these materials are extracted.

The effect from front ARC and back side reflection could also be simulated by adding corresponding command lines in the solving file of APSYS. The minority lifetime values for GaInP, GaAs and GaInAs are 20 ns, 100 ns and 3 ns, respectively. The recombination velocity for GaInP/AlGaAs interface is assumed to be $1.5x10^5$ cm/s[17], but is found having very minor influence to the modeling results.

4. RESULTS, ANALYSES AND DSICUSSION

A: GaInP/GaAs/Ge TJ cell

The simulation results for GaInP/GaAs/Ge TJ cell can be at first examined with the band diagrams. The band diagram at 3 volts is displayed in Fig. 3 (a), where we could see clearly how the band gap varies as the subcell goes from GaInP at the top (large distance in the figure) to Ge at the bottom. One could also notice the band diagram near the tunnel junctions where the conduction band electrons could be aligned with the valence empty states, as shown in Fig. 3 (b), an enlarged portion of the diagram shown in Fig. 3 (a).

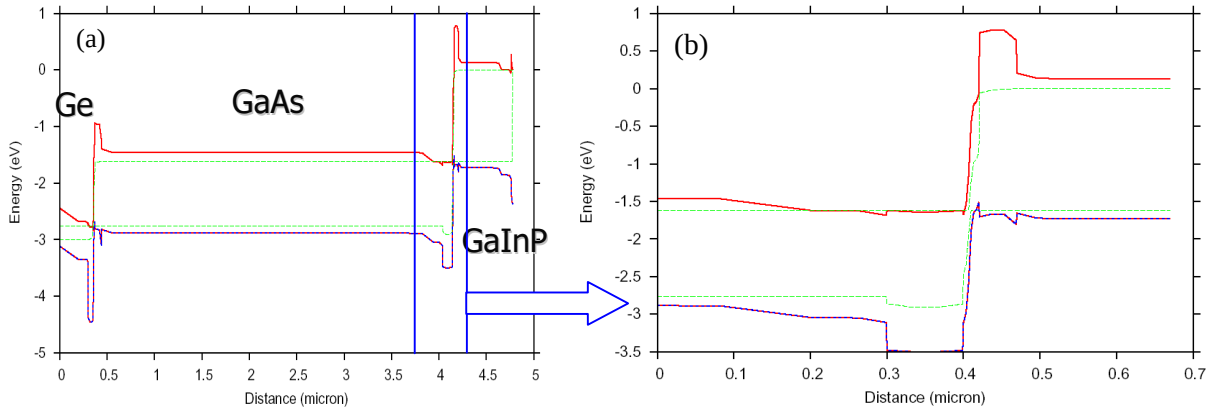

Fig. 3. (a) Band diagram of GaInP/GaAs/Ge TJ cell at 3 volts with solar irradiation and (b) an enlarged portion of the band diagram across a tunnel junction. The distance origin starts from the bottom and only part of the Ge base layer is shown.

The 2D relative energy density profile is also displayed in Fig. 4 (a), where the high energy illumination is mainly absorbed by the wide band gap GaInP subcell at the top and the medium energy illumination by the middle GaAs subcell whereas the low energy illumination by Ge subcell at the bottom. This is also reflected in the profile of optical generation rate, which is presented in Fig. 4 (b). Besides these results displayed, other physical properties like electron and hole concentrations, electric field and potential, quantum efficiency, and current density etc can also be obtained.

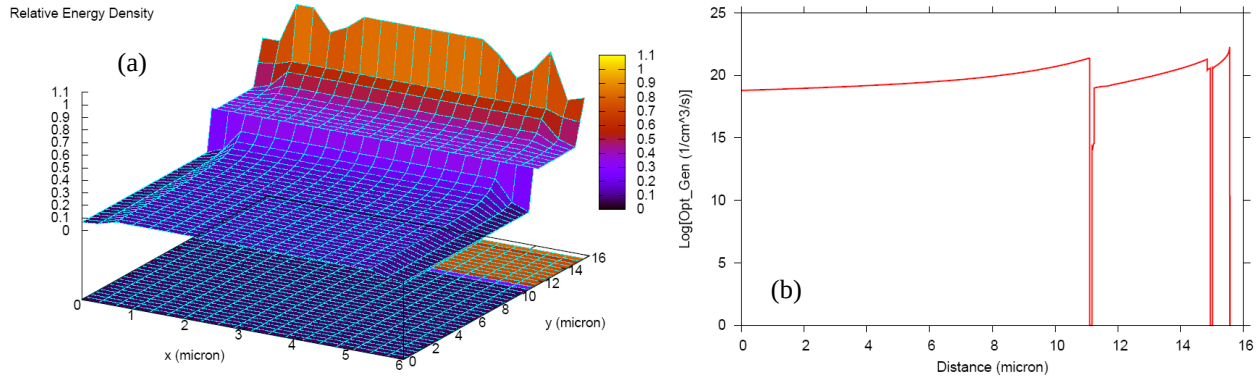

Fig. 4. (a) 2D relative energy density profile, and (b) optical generation rate for the GaInP/GaAs/Ge TJ cell simulated.

The simulated short-circuit current density is also compared with the experimental results and presented in Fig. 5. The result is in agreement with the experimental on all the aspects from the current magnitude, the curve shape to the open-circuit voltage. The modeled cell efficiency is about 29.4%, a little bit higher than the experimental one. The difference might be attributed to the actual-size device series resistance involved in the experimental measurement. The actual cell

size information together with series resistance was missing in Ref. 17 and it is not included in the modeling. Nevertheless, our modeling results are also comparable with the results shown in Ref. 16, where a different simulator has been used.

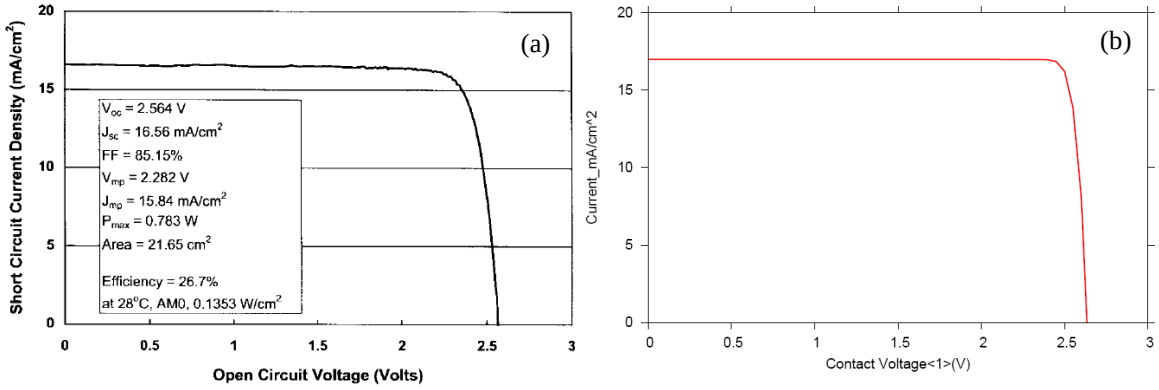

Fig. 5. IV curves: (a) experimental result[17] and (b) simulated result for the GaInP/GaAs/Ge TJ cell by Crosslight APSYS.

Current matching analysis is an important technique for solar cell design optimization. Our simulation results indicate that the top and the middle subcells are slightly mismatched (matched within 10%) with the short-circuit current for the GaInP/GaAs/Ge TJ cell modeled above. This is shown in Fig. 6 where we can see that the middle GaAs subcell is current limiting. There seems to be no much space for further current-matching optimization with the top and the middle subcells as the mismatch is within 10%. On the other hand, we could see that the short-circuit current for Ge subcell is very high and much of this component is just wasted due to the current limiting of the middle subcell. It should be also mentioned that the current matching analyses also depend on the solar spectra as well as the ARC layer configuration. We have used MgF_2(130 nm)/ZnS(65 nm) as our best guess for ARC when making the current matching modeling for Fig. 6.

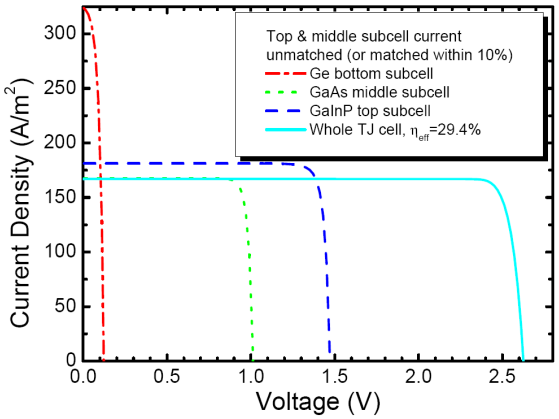

Fig. 6. I-V curves for subcells and the whole GaInP/GaAs/Ge TJ cell simulated by Crosslight APSYS. The modeling assumes front ARC layers MgF_2(130 nm)/ZnS(65 nm).

It may be also interesting to study how the doping density for the main absorber layer will affect the cell performance. Take the middle GaAs subcell as an example, and we change the p-GaAs layer doping density. This will mainly affect the minority-carrier lifetime as well as the mobility for p-GaAs absorber layer. Assuming that the minority carrier (electron) lifetime is related with the p-doping density N_{pGaAs} (in m^{-3}) as $\tau=10^{16}/N_{pGaAs}$ (τ in s)[24], we have simulated the I-V curves and cell efficiency with various p-GaAs layer doping density. The results are shown in Fig. 7 (a) for I-V curves and in Fig. 7 (b) for cell efficiency. The lower the p-GaAs layer doping density is, the higher the electron lifetime will be. This results in higher short-circuit current and higher efficiency.

The quantum efficiency (QE) is an important characteristic for solar cell. Crosslight APSYS could also manage to simulate it although the accuracy of the result depends on the compiled material index files, the ARC layer(s) and the solar spectra utilized. The accurate modeling of the QE is currently under way and will be presented later elsewhere.

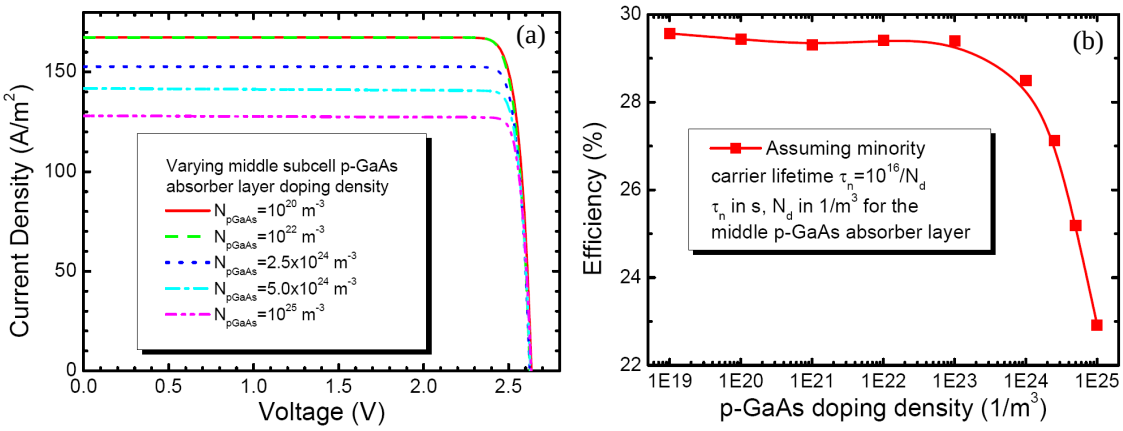

Fig. 7. (a) I-V curves for the GaInP/GaAs/Ge TJ cell with various middle subcell p-GaAs absorber layer doping density and (b) TJ cell efficiency versus p-GaAs doping density.

Significant efforts have been devoted to improve the cell efficiency during the past two decades. Several reports[6,7,25] indicate that using metamorphic material is a feasible approach to increase the cell efficiency. Taking the lattice-mismatched, or metamorphic subcell material like unconventional ternary alloy GaInNAs for solar cells with more than triple junctions, was investigated to achieve the goal with 40% or higher solar cell efficiency[25]. In the following sub-section, we will present some modeling results on the inverted-grown metamorphic GaInP/GaAs/GaInAs TJ cell.

B: Metamorphic GaInP/GaAs/GaInAs TJ cell

The band diagram at open circuit condition is given in Fig. 8 (a). The band discontinuities at the hetero-interfaces, and the broken band at the tunnel junctions are clearly shown. The quasi-Fermi levels for electron and holes are also depicted, and from which the V_{oc} at each subcell can be obtained. The three subcell V_{oc} values sum up to the total open circuit voltage for the whole cell. The vector current flow plot is also shown in Fig. 8 (b) at bias near V_{oc}. The 2D nature of current flow is seen clearly.

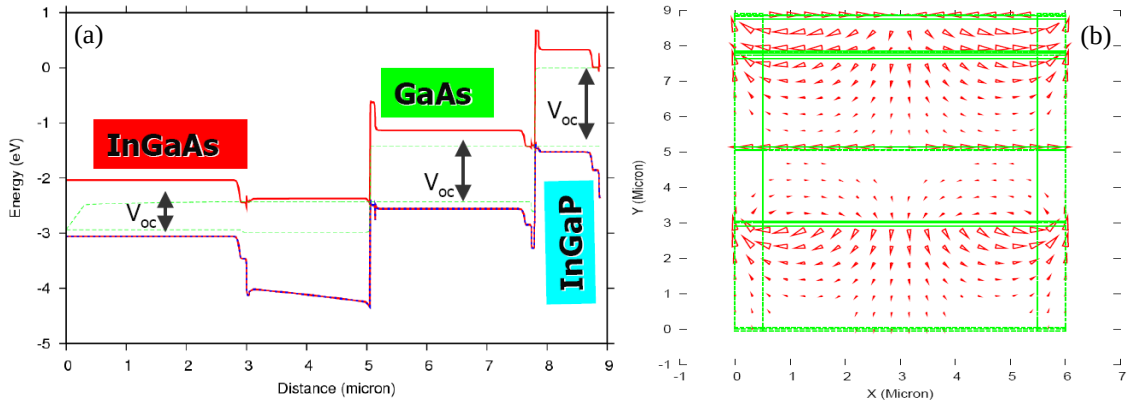

Fig. 8. (a) Energy band diagram at open circuit condition, and (b) vector current flow biased close to V_{oc}.

Fig. 9 (a) shows the relative light power density along the vertical direction. Slight fluctuations at the interfaces are due to the interferences of light wave calculated by transfer matrix method. We see that light power drops about 25% across the top GaInP subcell, while GaAs subcell absorbs only about 10% of the light power, and the majority of the light is absorbed by the bottom GaInAs subcell. Only about 13% light power is unused. With the layer thicknesses given by Geisz et al[6], the current density of three subcells are mismatched within 10% as shown in Fig. 9 (b), and the GaAs subcell is the current limiting. For the current mismatched (within 10%) case, the I-V curve for the whole TJ cell shown in Fig. 9 (b) is in good agreement with the experimental. The three characteristic values for short-circuit current (I_{sc}), open-circuit voltage (V_{oc}) and conversion efficiency are compared in Table 1 with the experimental.

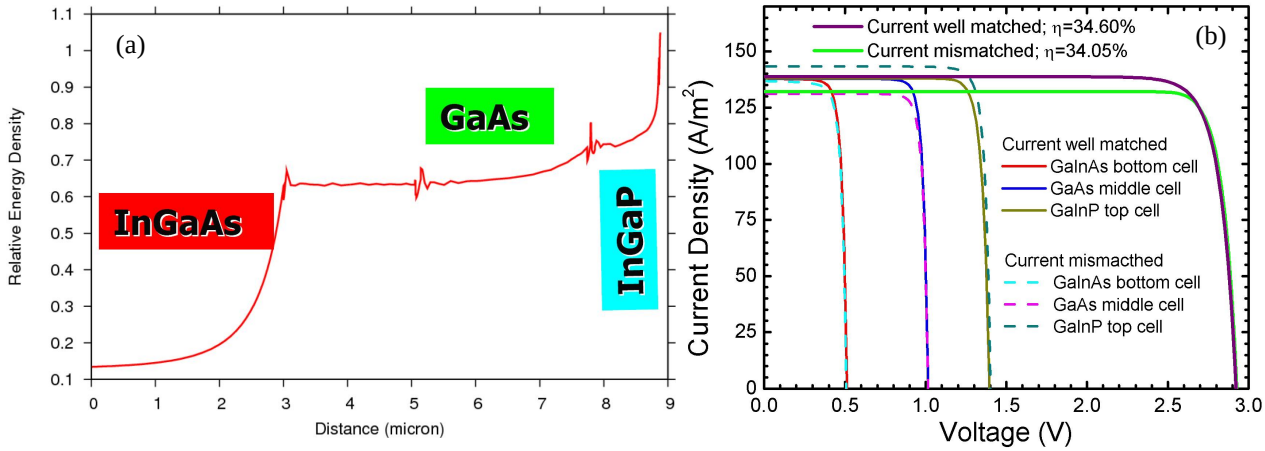

Fig. 9. (a) Relative light power density along vertical direction, and (b) I-V curves for subcells and for the whole TJ cell shown when current density is mismatch (within 10%) and is well matched.

Table 1. Comparison between the modeling results and the experimental[6].

	V_{oc} (V)	I_{sc} (mA/cm^2)	Efficiency (%)
Experimental	2.96	13.1	33.8
Modeling	2.93	13.2	34.1

The device structure design can be further optimized by detailed current matching analyses. Fig. 10 (a) and (b) show how subcell thickness can be adjusted to achieve good current matching among all the three subcells. When well matched, the TJ cell I_{sc} can be improved to about 13.9 mA/cm^2, leading to cell efficiency enhanced to about 34.6%, as displayed in Fig. 9 (b). Again the detailed current matching modeling depends on ARC layer configuration and thickness, the specific solar spectra used as well as the accuracy of the specific cell material index files[21-23].

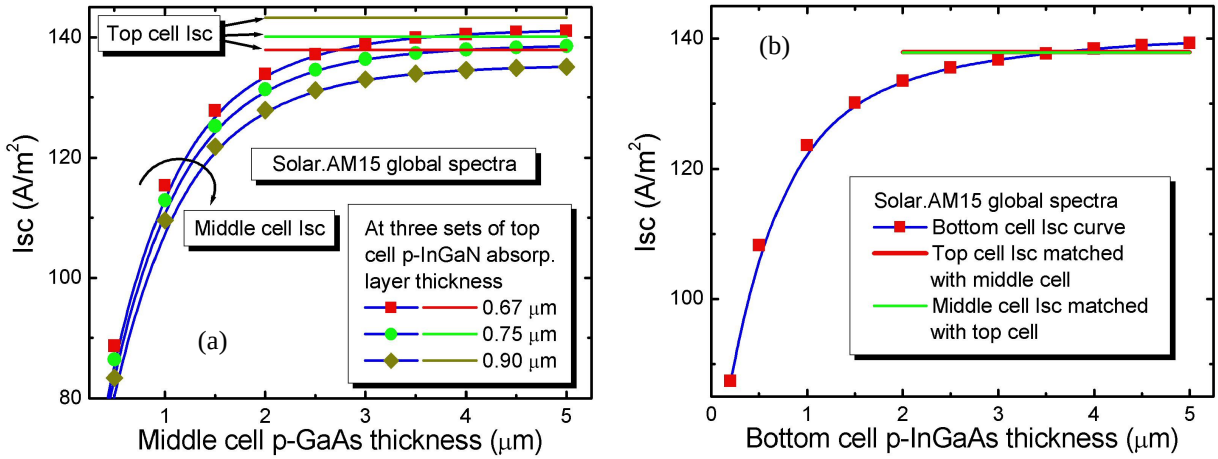

Fig. 10. (a) Achieving current matching between the top and middle subcells, and (b) achieving current matching among all the three subcells.

It is interesting to investigate the TJ cell behavior versus multi-sun concentrations. Fig. 11 shows that V_{oc} increases logarithmically with concentration. The fill factor, as shown in Fig. 12 (a), increases initially with concentration, but decreases significantly when sun number is larger than ~80. Correspondingly the efficiency, as shown in Fig. 12 (b), shows an optimal point with highest value versus concentration. After that optimal point, the efficiency will decrease. The reduction of efficiency as well as the fill factor at high concentration sun number is due to the enhanced limiting effect of the series resistance[6,18], which can be observed from the I-V curves shown in the inset of Fig. 12 (a).

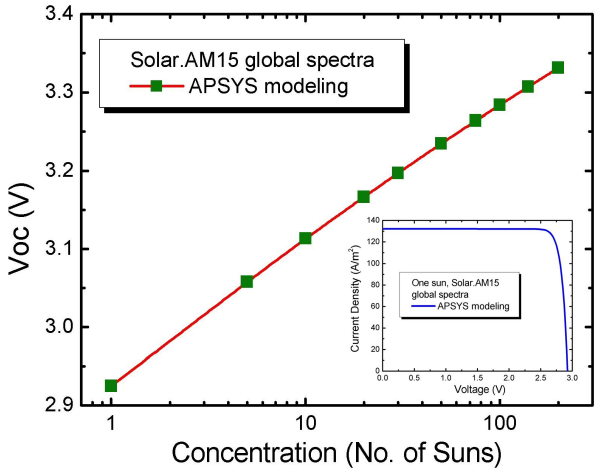

Fig. 11. V_{oc} versus concentration (inset: one-sun I-V curve).

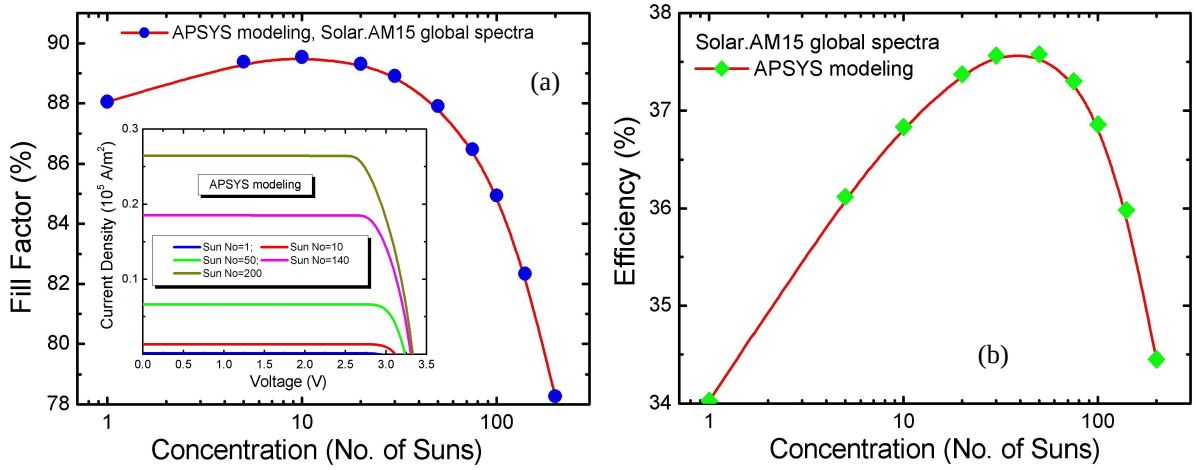

Fig. 12. (a) Fill factor versus concentration (inset: multi-sun I-V curves), (b) conversion efficiency versus concentration.

The modeling results shown above assume that the front metal contact pads have no shading and reflection effect. It is, however, interesting to consider the more realistic case with front metal pad reflection and to study the effect of the top contact grid spacing and its relative covered ratio. In Fig. 13 (a), efficiency versus concentration is plotted at various separation distances between top contact pads. At different separation distance, the series resistance starts to play significant role at different concentration sun number. But the top contact grid density also limits the efficiency. The narrower the contact pad separation is, the higher the relative covered ratio by the top contact grid. This indicates that the optimal concentration point with highest efficiency varies depending on the top contact grid separation as well as on the contact grid density. Wide separation distance reduces the contact grid density and leads to the reduced reflection and shading effect, which improves the efficiency. But wide separation distance can also make the series resistance more effective at a smaller concentration sun number to limit the efficiency, which supposes to be enhanced by the concentration effect. There is apparently a trade-off for the cell design consideration.

This is also elaborated in Fig. 13 (b), where curves for the efficiency at fixed sun number (200) and the optimal concentration sun number are plotted versus the relative ratio covered by the front contact pads. With the front contact pad separation increasing (correspondingly, the relative ratio covered by the front pads decreasing), the optimal sun number, with which highest efficiency can be achieved, decreases. This is also shown in Fig. 13 (a). At fixed sun number, there is an optimal point with highest efficiency for the relative ratio covered by the front contact pads. These results indicate that the realistic solar cell design is a complex task with many factors to be taken into consideration. Crosslight APSYS apparently provides a very useful tool kit in this regard.

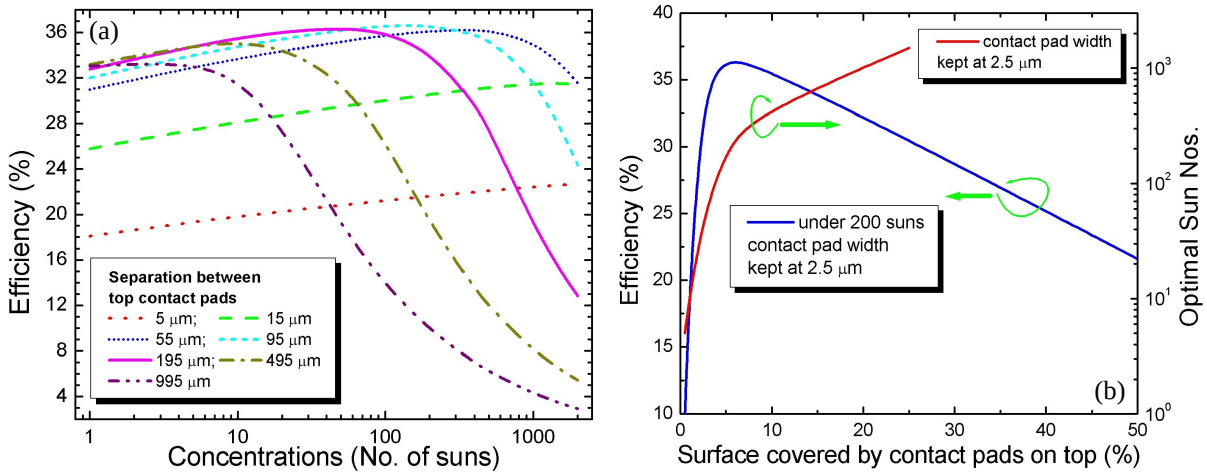

Fig. 13. (a) Conversion efficiency versus concentration at various separation distances between top contact pads, and (b) conversion efficiency and optimal sun number versus relative ratio covered by contact pads on top. The contact pad (grid) width is kept at 2.5 μm. Relative ratio is derived versus different separation distance between contact pads.

C: Discussion

The GaInP/GaAs/Ge TJ cell and the metamorphic GaInP/GaAs/GaInAs TJ cell mentioned above are modeled with Solar.AM0 and AM1.5G spectra respectively. In order to make comparison with these two TJ cells, we have re-simulated the metamorphic GaInP/GaAs/GaInAs TJ cell with Solar.AM0 and ARC as MgF_2(130 nm)/ZnS(65 nm). The simulated I-V curves for individual subcells and whole TJ cell are presented in Fig. 14. The cell efficiency is close to what is reported (30.6±0.9) for AM0 spectra[6], but is 4.8% lower than the one as shown in Table 1 when simulated with AM1.5G and optimized ARC. As compared with Fig. 9 (b), the three subcells are apparently mismatched (over 10%) with the short-circuit current density when the solar spectra and the ARC changed. The middle GaAs subcell is still current limiting.

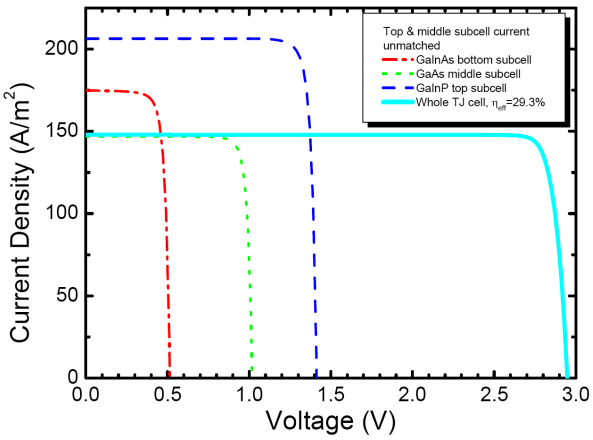

Fig. 14. I-V curves for subcells and the whole GaInP/GaAs/Ge TJ cell simulated by Crosslight APSYS. The modeling results shown in this figure assumes front ARC layers MgF_2(130 nm)/ZnS(65 nm) and Solar.AM0 spectra.

Comparing with Fig. 6 for the GaInP/GaAs/Ge TJ cell, the cell efficiency is almost the same but with lower short circuit current density and larger open circuit voltage. The large V_{oc} is due to the high band gap for the bottom GaInAs subcell comparing to Ge bottom subcell in Fig. 6. For GaInP/GaAs/Ge TJ cell, since the Ge bottom subcell shows high short-circuit current, the concern of current matching is mainly with the middle and the top subcells. For the metamorphic GaInP/GaAs/GaInAs TJ cell, due to limited absorption of the bottom GaInAs subcell, the concern for current matching is mainly with the bottom and the middle subcells, as shown both in Fig. 9 (b) and Fig. 14. The question is whether the

metamorphic GaInP/GaAs/GaInAs TJ cell can achieve the same short-circuit current density (~166 A/m^2 under Solar.AM0) as that of the GaInP/GaAs/Ge TJ cell whereas maintaining a large V_{oc} as this indicates significant enhancement of the conversion efficiency. The answer is probably negative because any increment for the short-circuit current of the middle GaAs subcell will likely result in the reduction of the short-circuit current of the bottom GaInAs subcell. In certain circumstances, the bottom GaInAs subcell becomes current limiting. Anyway, for the metamorphic GaInP/GaAs/GaInAs TJ cell, our modeling results in both Fig. 14 and Fig. 9 (b) indicate that the top GaInAs cell may be a little thick from current matching analyses.

Modeling work especially on the influence of ARC to the TJ cell performance is currently under way. Contour plots of cell short-circuit current with various ARC configuration should give a better prediction of the optimized cell performance[7,26] with optimized ARC layers although optimization depends on the specific solar spectra used for irradiation. More sophisticated consideration for incorporating thermal effect is also under way.

5. SUMMARY

In summary, based on the advanced drift and diffusion theory with improved tunneling junction model, 2D modeling for the GaInP/GaAs/Ge and the inverted-grown metamorphic GaInP/GaAs/GaInAs TJ solar cells are performed by using a commercial software, the Crosslight APSYS. Basic physical quantities like band diagrams, optical absorption and generation are obtained and characteristic results such as I-V curves, current matching, fill factors, efficiencies etc under one-sun and multi-sun illumination condition are presented. Some of the modeling results generally agree with the published experimental results for both TJ cells. Comparative analyses are made with these two TJ cells and optimization approaches are discussed with respect to minority carrier lifetime, front ARC configuration, and the top contact grid size and spacing. The comprehensive models together with various applicable features make Crosslight APSYS a powerful tool kit to simulate photosensitive and other advanced semiconductor devices.

ACKNOWLEDGMENT

We appreciate Michel Lestrade for some technical help.

REFERENCES

1. J. M. Olson, S. R. Kurtz, A. E. Kibbler, and P. Faine, "A 27.3% efficient $Ga_{0.5}In_{0.5}P$/GaAs tandem solar cell," *Appl. Phys. Lett.* 56, pp. 623-625 (1990).
2. D. J. Friedman, S. R. Kurtz, K. A. Bertness, A. E. Kibbler, C. Kramer, J. M. Olson, D. L. King, B. R. Hansen, and J. K. Snyder, "GaInP/GaAs monolithic tandem concentrator cells," in *Proc. 1st World Conf. PVEC*, p. 1829 (1994).
3. M. J. O'Neill, A. J. McDanal, M. F. Piszczor, M. I. Eskenazi, C. Carrington, D. L. Edwards, and H. W. Brandhorst, "The stretched lens ultralight concentrator array," *28th IEEE PVSC*, pp. 1135-1138 (2000).
4. M. J. O'Neill, A. J. McDanal, H. L. Cotal, R. Sudharsanan, D. D. Krust, J. H. Ermer, N. H. Karam, D. R. Lillington, "Development of terrestrial concentrator modules incorporating high efficiency multi-junction cells," *28th IEEE PVSC*, pp. 1161-1164 (2000).
5. M. Yamaguchi et al., "Japanese activities of R&D on III-V concentrator solar cells and modules," *19th European Photovoltaic Solar Energy Conference*, pp. 2014-2017 (2004).
6. J. F. Geisz, S. Kurtz, M. W. Wanlass, J. S. Ward, A. Duda, D. J. Friedman, J. M. Olson, W. E. McMahon, T. E. Moriarty, and J. T. Kiehl, "High-efficiency GaInP/GaAs/InGaAs triple-junction solar cells grown inverted with a metamorphic bottom junction," *Appl. Phys. Lett.* 91, pp. 023502-1-023502-3 (2007).
7. R. R. King, D. C. Law, K. M. Edmondson, C. M. Fetzer, G. S. Kinsey, H. Yoon, R. A. Sherif, and N. H. Karam, "40% efficient metamorphic GaInP/GaInAs/Ge multijunction solar cells," *Appl. Phys. Lett.* 90, pp. 183516-1-183516-3 (2007)
8. Spectrolab's product data sheets, http://www.spectrolab.com/prd/terres/cell-main.htm
9. Crosslight APSYS 2008 and technical manuals, Copyright © Crosslight Software Inc. (2005).
10. Z. Q. Li and Simon Z. M. Li, "Sophisticated models replicate the effects of tunnel junctions," *Compound Semicond.* 13, pp. 29-31 (2007).
11. E. O. Kane, "Zener tunneling in semiconductors," *J. Phys. Chem. Solids* 12, pp. 181-188 (1960).
12. C. B. Duke, *Tunneling in Solids*, Ch. 4, Copyright © Academic Press, New York (1969).

13. J. L. Moll, *Physics of Semiconductors*, Ch. 12, Copyright © McGraw-Hill, New York (1964).
14. P. Yeh, *Optical Waves in Layered Media*, Copyright © John Wiley & Sons Inc., (1988).
15. PC1D, www.pv.unsw.edu.au/links/products/pc1d.asp
16. S. Michael, "A novel approach for the modeling of advanced photovoltaic devices using SILVACO/ATLAS virtual wafer fabrication tools," *Solar Energy Materials & Solar Cells* 87, pp. 771-784 (2005).
17. N. H. Karam, R. R. King, B. T. Cavicchi, D. D. Krut, J. H. Ermer, M. Haddad, L. Cai, D. E. Joslin, M. Takahashi, J. W. Eldredge, W. T. Nishikawa, D. R. Lillington, B. M. Keyes, and R. K. Ahrenkiel, "Development and characterization of high-efficiency $Ga_{0.5}In_{0.5}P$/GaAs/Ge dual- and triple-junction solar cells," *IEEE Trans. Electron. Dev. 46*, pp. 2116-2125 (1999).
18. S. M. Sze, *Physics of Semiconductor Devices*, Copyright © John Wiley & Sons, Inc (1981).
19. M. P. Thekaekara, "Data on incident solar energy," *Suppl. Proc. 20th Annu. Meet. Inst. Environ. Sci*., p. 21 (1974).
20. Source NREL web page, http://rredc.nrel.gov/solar/spectra/am1.5/
21. R. Ferrini, G. Guizzetti, M. Patrini, A. Parisini, L. Tarricone, and B. Valenti, "Optical functions of InGaP/GaAs epitaxial layers from 0.01 to 5.5 eV," *Eur. Phys. J. B* 27, pp. 449-458 (2002).
22. S. L. Chuang, *Physics of Optoelectronic Devices*, Copyright © 1995 by John Wiley & Sons Inc.
23. Online semiconductor materials parameters, http://www.ioffe.rssi.ru/SVA/NSM/Semicond
24. *Properties of Gallium Arsenide*, Eds. B. R. Brozel and G. E. Stillman, published by INSPEC (1996).
25. R. R. King, R. A. Sherif, G. S. Kinsey, S. Kurtz, C. M. Fetzer, K. M. Edmondson, D. C. Law, H. L. Cotal, D. D. Krust, J. H. Ermer, and N. H. Karam, "Bandgap engineering in high-efficiency multijunction concentrator cells," *Inter. Conf. Solar Concentrators Generat. Electricity Hydrogen*, 1-5 May 2005, Scottside, Arizona.
26. J. M. Olson, D.J. Friedman, and S. Kurtz, "High-efficiency III-V multijunction solar cells," in *Handbook of Photovoltaic Science and Engineering*, Edited by A. Luque and S. Hegedus, Copyright © 2003 John Wiley & Sons, Ltd.